

Chapter 14

Micromechanical Evidences on Interfibre Failure of Composites

Federico París, Elena Correa, and Vladislav Mantič

14.1 Introduction

Composite materials have been presented from the very beginning as non-isotropic, being this its main characteristic. This fact certainly plays a key role from a structural point of view when designing in terms of a required level of stiffness or when evaluating the distributions of stresses with a stacking sequence involving plies with different orientations of the fibres.

However, the non-isotropic character of a lamina is irrelevant from a failure point of view, the important question when damage or failure is under consideration is the non-homogeneous character of composite materials.

When revising classical books on composites, see Jones [1], Tsai and Hahn [2], Agarwal and Broutman [3] or Halpin [4], among many others, there is a vast part of them impregnated of the non-isotropic character of the material, whereas only a small part is associated with the non-homogeneous constitution of composites. Micromechanics has been the word traditionally used to recognize the non-homogeneous character of a composite. However, the micromechanic parcel has been usually associated with the predictions of stiffness or strength properties of the composite as a function of the properties of the constituents, fibre and matrix.

It is also remarkable that when generating the failure criteria of composites, a big emphasis was put originally in adapting existing failure criteria to the non-isotropic character of the material, rather than recognizing the internal structure, the non-homogeneous character of composites.

F. París (✉) • E. Correa • V. Mantič
Elasticity and Strength of Materials Group, School of Engineering, University of Seville,
Camino de los Descubrimientos, s/n 41092-Seville, Spain
e-mail: fparis@us.es; ecorrea@us.es; mantic@us.es

Likewise, it is an extended idea between final designers of aeronautical components made of composites, that Micromechanics is a beautiful subject from an academic point of view, yet irrelevant when designing an actual structure.

When the necessity of improving the performance of composites required a better knowledge of the mechanisms of damage and modes of failure, a significant attention to micromechanics as a key to understand the failure of composites, in order to avoid non-physically based failure criteria, París [5], was devoted.

This chapter presents a summary of the micromechanics analysis carried out by the authors from the Group of Elasticity and Strength of Materials of the School of Engineering at the University of Seville, intending to give an explanation on different facts observed at meso- or macro-level, getting confidence on the capacity of Micromechanics to generate physically based failure criteria. The studies presented are referred to what is known as interfibre failure, a failure not dominated by the fibres which may involve debonding between fibres and matrix as well as breakage of the matrix.

First, Sect. 14.2, a very brief summary of the tools used in the studies carried out, is presented. Then, Sect. 14.3, a case illustrating the capacity of Micromechanics to understand the behaviour of composites is studied. The capacity of the stress vector used in many failure criteria to predict the interfibre (or matrix) failure is investigated based on Micromechanics. In Sect. 14.4 the morphology of the interfibre failure under tension and compression is studied, including the presence of a secondary transversal stress. Section 14.5 is devoted to understand a particular case of behaviour of composites under fatigue loading: the increase of damage under compression excursions in the fatigue cycles. Section 14.6 is devoted to the role of residual stresses at micromechanical level originated during curing cycle due to the mismatch between the expansion coefficients of fibre and matrix. Finally in Sect. 14.7, two relevant topics are considered: one is the presence of additional fibres surrounding the one under study, and the second is the role of Micromechanics in understanding the *scale effect* in composites.

14.2 Tools

Damage at micromechanical level is mainly characterized by the presence of cracks. Some of them run through the matrix, their growth being controlled by Linear Elastic Fracture Mechanics (LEFM) associated with an isotropic medium, therefore not requiring any special attention in this chapter.

However, the initiation of the interfibre damage is associated with a debonding between fibre and matrix, giving rise to a crack controlled by Interfacial Fracture Mechanics (IFM), which uses similar concepts, to those employed in LEFM, Stress Intensity Factors (SIF) and Energy Release Rate (ERR).

Interface cracks or cracks between dissimilar materials present a much more complicated behaviour as those in an isotropic linear elastic medium. There are two models to analyse interfacial cracks: *the open model* and the *contact model*.

In the open model, Williams [6], the interface crack is assumed to be open (with traction-free crack faces), whereas in the contact model, Comninou [7], the faces near the crack tip are assumed to be in contact under the load application.

None of the two models is free of inconsistencies and/or difficulties in its application. Thus, in the open model, oscillations and interpenetrations appear near the crack tip indicating the necessity of having a contact zone. On the contrary, when the contact model is used, although the solution obtained with this model is strictly speaking the only one physically correct, the size of the contact zone may be so small that is not coherent with a continuum representation of the material.

Having these limitations in mind, there are situations where only one of these models can be considered adequate, but there are also cases, like those appearing in the studies carried out in this chapter, where both models are required along the fracture process. Thus, a switch from the open model to the contact model is required when analysing the growth of the fibre-matrix debonding.

An excellent example to clarify these questions is the one represented in Fig. 14.1, where it is shown a crack between dissimilar materials, one stiff, that can be associated with a fibre, and another compliant, that can be associated with the matrix. On the one side where the natural relative displacements coincide with the shear applied (left in the figure), a large contact zone will appear, whereas on the other side where the relative displacements of the lips are opposed to the shear applied (right in the figure), a bubble appears. Notice that a very small contact zone exists at this tip of the bubble, being represented in Fig. 14.1. Thus, the left-hand side of the crack would be controlled by a contact model approach whereas the right-hand side would be controlled by an open model approach.

A more detailed explanation on the application of these concepts into the study of interfibre failure of composites may be found in Mantič et al. [8], Paris et al. [9] and in Correa et al. [10], among others.

The debonding between fibre and matrix already presented is only a first phase of interfibre damage. As situations where a debonding crack abandons the interface and enters the matrix may appear in the study carried out, a criterion for the competition between an interface crack (the debonding crack between fibre and matrix) controlled by IFM and a regular crack (that penetrating into the matrix) controlled by LEFM is required.

The criterion used, represented in expression (14.1), is formulated in energetic basis, He and Hutchinson [11], where G^{int} is compared with G^{kink} , in terms of their ratios with respect to the corresponding critical values.

$$\frac{G^{\text{int}}}{G_c^{\text{int}}} > \frac{G^{\text{kink}}}{G_c^{\text{kink}}} \Rightarrow \text{extension}, \quad \frac{G^{\text{int}}}{G_c^{\text{int}}} < \frac{G^{\text{kink}}}{G_c^{\text{kink}}} \Rightarrow \text{kink} \quad (14.1)$$

The values of the toughness associated with a bimaterial system strongly depend on the mixity ψ_k . In this study, the critical value of the energy associated with the interfacial crack will be evaluated, when required, by means of expression (14.2),

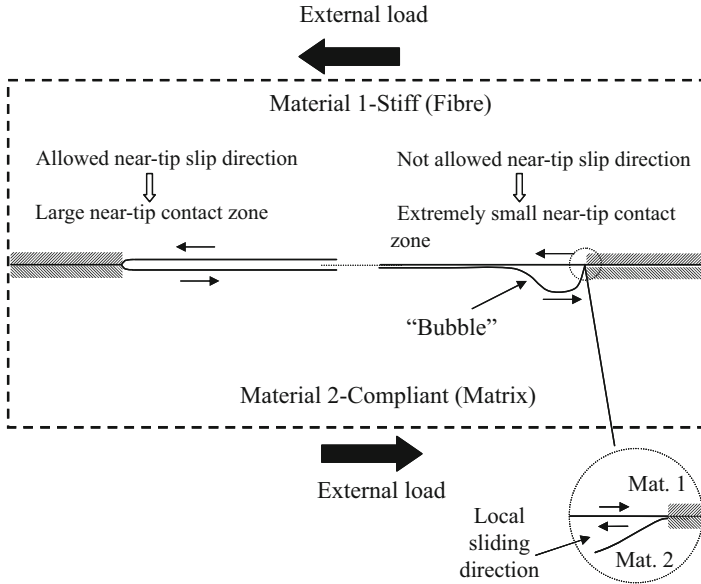


Fig. 14.1 Morphology of a crack between dissimilar materials under shear external load

Hutchinson and Suo [12], with reference to the critical value of G associated with mode I.

$$G_C^{int}(\psi_k) = G_{IC}^{int}[1 + \tan^2(1 - \lambda)\psi_k] \tag{14.2}$$

where G_{IC}^{int} is the toughness associated with mode I and λ is a material parameter.

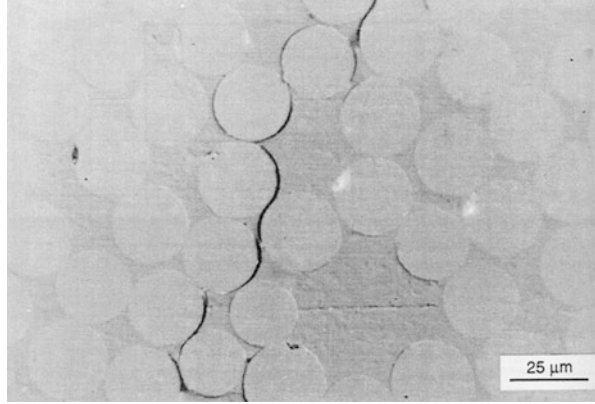
Finally, the numerical tool used to perform the micromechanical analysis will be the Boundary Element Method (BEM), París and Cañas [13]. The reason for this choice is that BEM is specially equipped for dealing with problems involving non-linear conditions along the boundary (contact between the lips of a crack) and with singular values of the stresses (associated with the presence of a crack), the high accuracy obtained in the predictions being also remarkable.

14.3 Micromechanics to Understand Interfibre Failure

The problem under consideration can be clearly illustrated by means of Fig. 14.2, Gamstedt [14], which corresponds to a glass fibre system.

The objective of this section is to illustrate how a micromechanical analysis of fibre-matrix debonding can explain a question associated with interfibre failure prediction. Many criteria for this failure take as reference the stress vector associated with the plane of failure, see, for instance, Hashin and Rotem [15], Puck and

Fig. 14.2 Fibre-matrix debonds under transversal load



Schürmann [16] and Sun et al. [17]. The original idea of Hashin would have led, for a 3D stress state, to the following criterion:

$$\left(\frac{\sigma_n}{Y_c}\right)^2 + \left(\frac{\tau_{nl}}{S}\right)^2 + \left(\frac{\tau_{nt}}{S_T}\right)^2 = 1 \quad (14.3)$$

where σ_n , τ_{nl} and τ_{nt} are, respectively, the components of the stress vector, normal to the plane (σ_n), tangent to the plane in the direction of the fibre (τ_{nl}) and tangent to the plane transverse to the fibre (τ_{nt}). The denominators correspond to the allowables of the components of the stress vector.

This equation was maintained for tension and modified for the failure under compression. The important thing in any case is that all this family of interfibre failure criteria did not involve other components of the stress state different from those included in the stress vector associated with the plane of failure. Thus, with reference to the two-dimensional case represented in Fig. 14.3a, only components σ_{22} and σ_{23} would be involved in the failure, whereas no role on it would be assigned to the component σ_{33} . However, a detailed view of the failure described in Fig. 14.3b indicates that the debonding between fibre and matrix might be affected by the presence of the component σ_{33} .

To analyse this question, a BEM model of a single fibre embedded in a matrix under a bidirectional stress state is going to be used, Fig. 14.4. This model allows a debonding crack to be considered, avoiding interpenetrations between fibre and matrix and giving the possibility of generating a contact zone between fibre and matrix, as indicated in Fig. 14.4. Notice that the model developed includes one symmetry plane, the angle θ_d represented in the figure being associated with one half of the total debonding crack. The properties of the materials used are specified in Table 14.1.

The ERR associated with the debonding crack is evaluated using the crack closure technique, expression (14.4), the crack growing from an angle α to $\alpha + \delta$ ($\delta \ll \alpha$)

$$G(\alpha) = \frac{1}{2\delta} \int_{\alpha}^{\alpha+\delta} \{(\sigma_{rr})_{\alpha}(u_r)_{\alpha+\delta} + (\sigma_{r\theta})_{\alpha}(u_{\theta})_{\alpha+\delta}\} d\theta \quad (14.4)$$

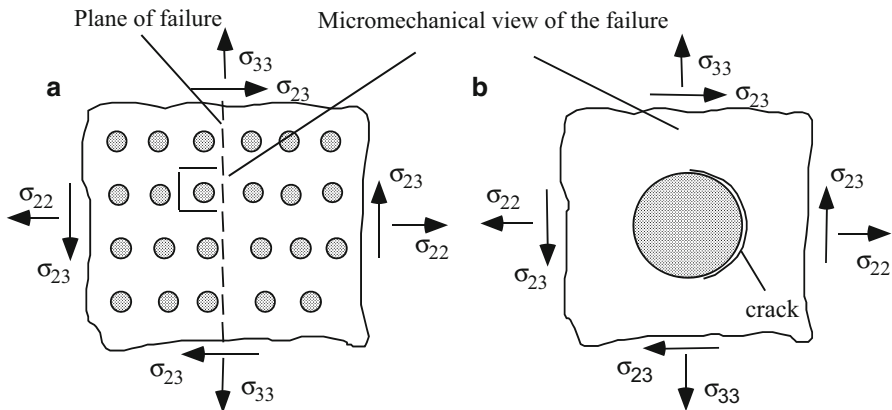


Fig. 14.3 Micromechanical implications of associating the failure at a plane with the components of the stress vector associated with such plane: (a) a general view, (b) single fibre view

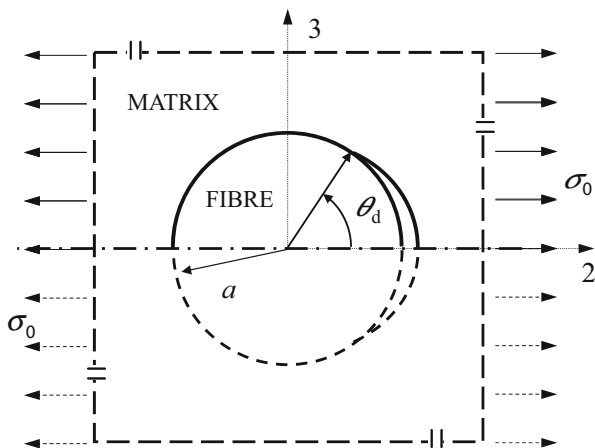


Fig. 14.4 Single fibre configuration with damage modelled by a debonding crack between fibre and matrix

Table 14.1 Elastic properties of fibre and matrix

Material	Poisson coefficient	Young modulus
Matrix (epoxy)	$\nu^m = 0.33$	$E^m = 2.79 \times 10^9 \text{ Pa}$
Fibre (glass)	$\nu^f = 0.22$	$E^f = 7.08 \times 10^{10} \text{ Pa}$

The evolutions of the ERR and their counterparts corresponding to modes I and II are shown, as a function of the debonding angle, in Fig. 14.5, for the particular case of having a single nominal stress. The values of G are calculated for different debonding angles (starting by a total 10° debonding) and are normalized by dividing the values of G by $G_0 = (1 + k^m/8\mu)\sigma_0^2\alpha\pi$ (Toya [18] and Murakami [19]), where $k^m = 3 - 4\nu^m$, μ is the shear modulus of the matrix and σ_0 denotes the value of the applied tension.

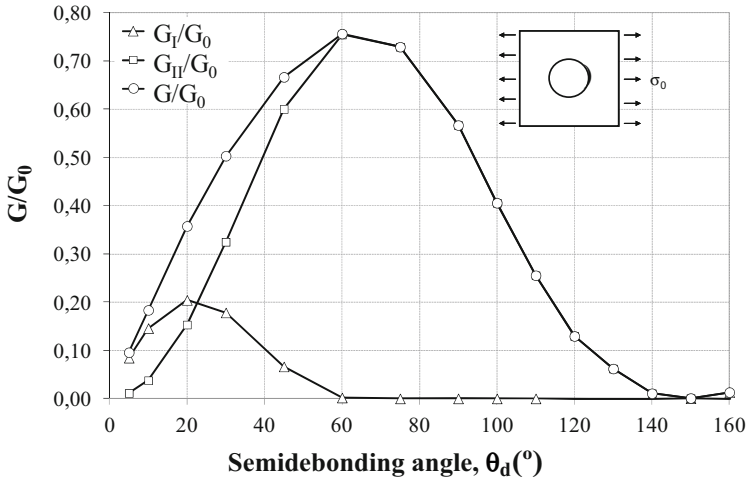


Fig. 14.5 Normalized total, G , and corresponding fracture modes parts, G_I and G_{II} , under tension normal to the plane of failure (case $T = 0$)

As can be clearly observed, mode I controls initial small debondings, as the crack is oriented almost perpendicular to the nominal stress. A mixed mode appears, with more preponderance of mode II as the crack progresses, reaching a pure mode II, with the generation of a contact zone, when the semidebonding angle reaches a value in the model of about 60° – 65° .

If a second nominal stress is applied, parallel to the plane of failure, then a clear alteration in the values of G is appreciated, see Fig. 14.6, where only the values of the total ERR are represented for simplicity. The values represented correspond to the case of a single tension ($T = 0$) versus the same tension with an additional compression parallel to the assumed plane of failure ($T = C$).

The presence of a compression parallel to the plane of failure produces a noticeable increment of G , which would lead to think that it produces an acceleration in the breaking procedure, the value of the breaking load decreasing in presence of a lateral compression. To check these predictions, experimental tests were conducted, París et al. [20], applying a tension normal to the fibres in a 90° specimen, with a lateral precompression. Notice that although the tension and the transverse compression are applied in the model at the same time, as the application of the compression involves a conforming contact problem, the two loads, compression and tension can be sequentially applied in the test for simplicity reasons, without altering the problem (assuming no friction is involved).

If it is assumed that the components of the stress vector control the interfibre failure, the ultimate strength of the specimen would not be affected by the presence of a lateral precompression. On the contrary, if the numerical BEM predictions are correct, then a significant decrease in the ultimate strength ought to be observed when increasing the lateral precompression.

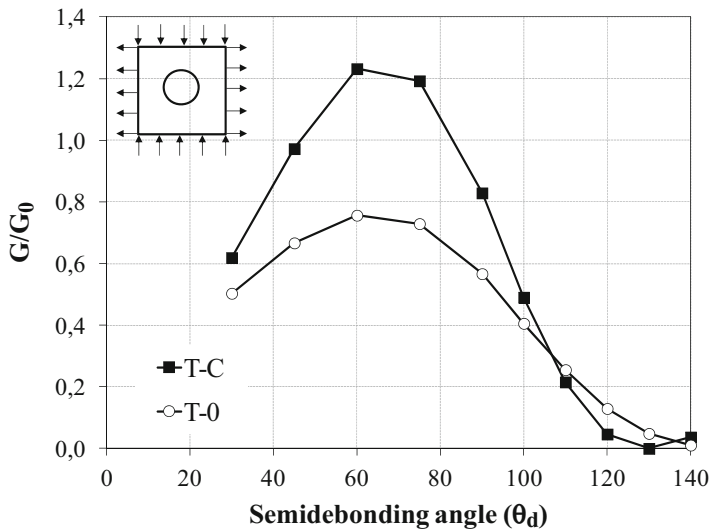


Fig. 14.6 Micromechanical implications of associating the failure at a plane with the components of the stress vector associated with such plane

The results, shown in Fig. 14.7, regardless of their noticeable scattering associated with a test performed under a load normal to the fibres and with the in-house design of the rig, clearly indicate the adequacy of the following assumption: due to the non-homogeneous character of the composite, the damage consisting on the debonding between fibre and matrix is clearly affected by components of the stress state not included in the stress vector.

The agreement between predictions based on micromechanics and the macroexperimental results makes us feel confident on the role that Micromechanics may play in helping to understand different aspects of the behaviour of composites, as will be shown in what follows.

14.4 Interfibre Failure

Once a particular question affecting the interfibre failure criteria of composites has been studied in the previous section, the complete morphology of the interfibre failure under tension and under compression is now going to be studied in detail, covering not only the debonding between fibre and matrix but also the complete failure of the lamina, always contemplated from a micromechanical point of view.

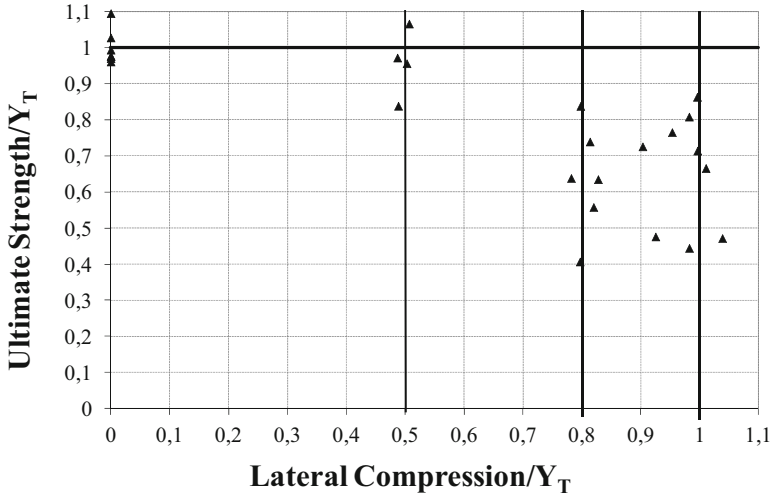


Fig. 14.7 Ultimate strength of the 90° specimen as a function of the lateral precompression applied

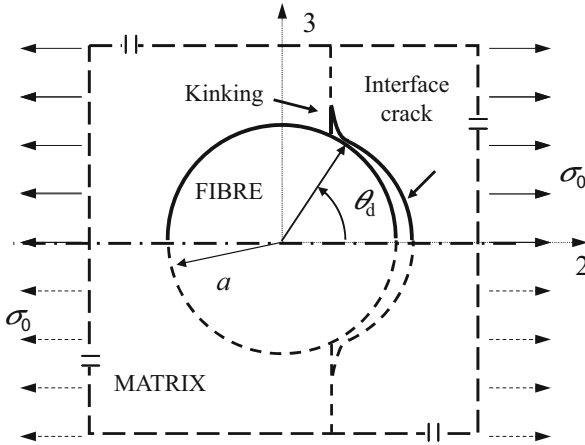


Fig. 14.8 Model of the damage in a single fibre under tension once the debonding crack kinks and penetrates into the matrix

14.4.1 Under Tension

In this section the configuration that is going to be analysed by BEM is shown in Fig. 14.8, which includes not only the debonding between fibre and matrix but also a potential abandon of the fibre-matrix interface, kinking into the matrix.

The first question to elucidate is the angle at which the debonding crack, considered to be the onset of the damage, may stop. To this end, both the values

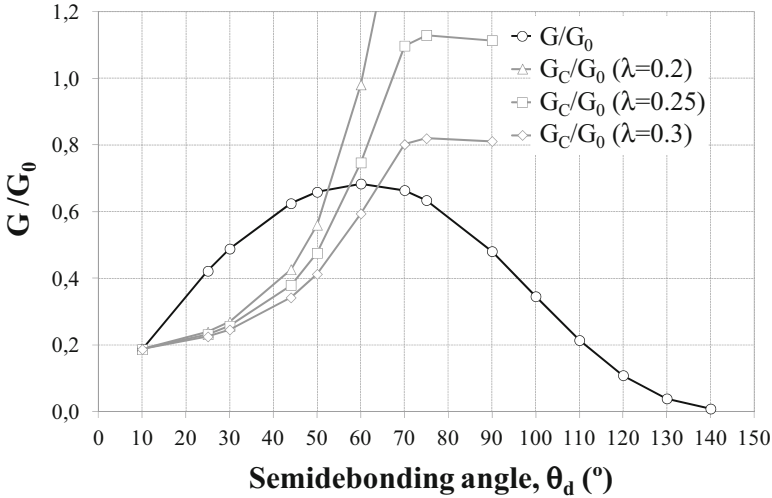


Fig. 14.9 Evolution of G and G_C as a function of the semidebonding angle

of the ERR G such as those associated with the toughness of the material, G_C , need to be known. As the mixity of the crack changes with the size of the debonding, it will be necessary to represent along with G the evolution of the values of G_C with the growth of the debonding, following the indications given in Sect. 14.2, as a function of a material parameter λ and the mixity ψ . An interesting discussion about the different options to represent the mixity can be found in Mantić and París [21] and París et al. [9], having chosen the mixity associated with G , ψ_G , in this study.

Figure 14.9 shows the evolution of G and G_C for different values of the parameter λ . It has been considered that the failure criterion ($G = G_C$) holds for a small semidebonding angle (10°).

The evolution appearing in Fig. 14.9 clearly shows that starting at a semidebonding of 10° , an unstable growth takes place, the crack stopping ($G_C > G$) for an interval between 55° and 65° , depending on the value of λ taken. Notice that the horizontal evolution of G_C observed is due to the appearance of a pure mode II, once a contact zone is generated.

Following on from the development of damage, once the crack stops, a competition between continuing the growth along the interface under a pure mode II in a stable way, and kinking and penetrating into the matrix, appears.

The possibility of kinking must be investigated under the light of a criterion, which in this case will be taken as the Maximum Circumferential Stress σ_θ , Erdogan and Sih [22]. Figure 14.10 reproduces the orientations of the directions associated with the maximum values of σ_θ for different positions of the debonding crack tip. A range is represented to cover the predictions for different values of the radius from the tip.

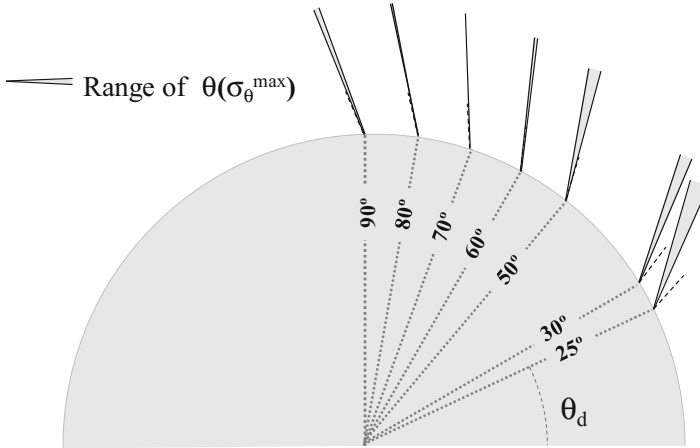


Fig. 14.10 Evolution, in the neighbourhood of the debonding crack tip, of the angle of maximum circumferential stress in the matrix

It can be clearly observed how in the range under interest (in the neighbourhood of 60°) the orientations of the maximum value of σ_θ correspond to an almost vertical direction, i.e., almost normal to the external applied load.

To elucidate now the question under consideration, this is, the progression of the damage, the values of the ERR G for both a debonding crack and a potential kinking crack (values corresponding to the vertical direction and those corresponding to the direction of maximum σ_θ are represented for completeness) are represented in Fig. 14.11.

The values of G associated with the kinking crack are, in the interval of interest, significantly greater than those associated with the debonding crack. Additionally, if the values of G associated with a kinked crack progressing into the matrix are represented, as shown in Fig. 14.12, it is clearly observed that, for obvious geometrical reasons, this growth will take place under mode I, which makes even more plausible the abandon of the crack of the interface to kink and penetrate into the matrix.

All of the above lead to consider that the growth of the damage could be visualized by the scheme shown in Fig. 14.13, under the acronym $T - 0$. The influence of the presence of another transverse load is also represented in Fig. 14.13 under the acronym $T - 0.5T$ for the case of the superposition of a transverse tension with a value of one half of the reference tension, and under the acronym $T - C$ for the case of the superposition of a transverse compression with the same value than of the reference tension.

In general terms, it can be observed that the main alterations when a secondary transverse load appears in a failure dominated by tension occur in the interface crack growth, in particular, this growth could be larger for the $T - nT$ cases and slightly smaller for the $T - nC$ situations. Kinking towards the matrix seems not

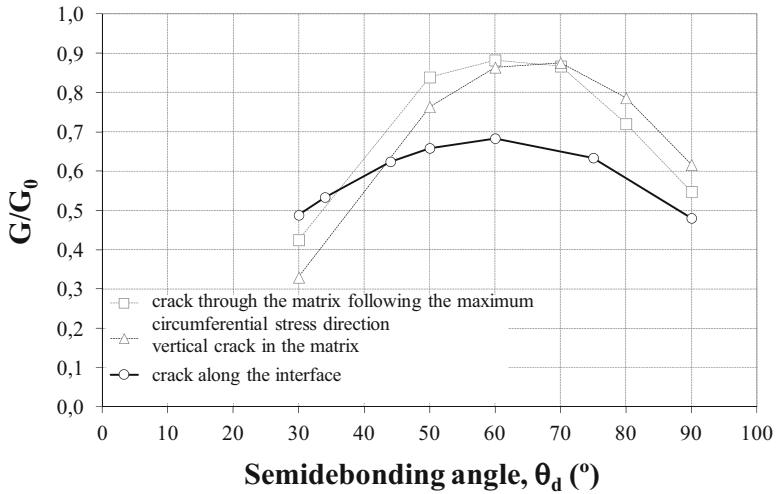


Fig. 14.11 Values of G for the debonding crack continuing the growth along the interface and values of G for a potential kinking crack as a function of the semidebonding angle

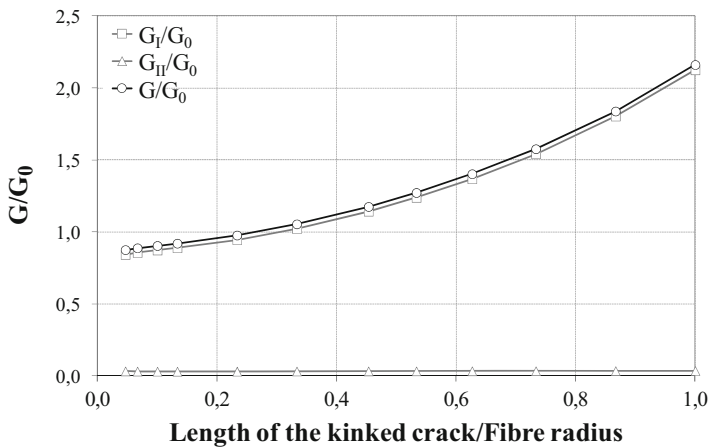


Fig. 14.12 Values of G for a kinked crack progressing into the matrix in a vertical direction

to be remarkably affected by the presence of the secondary load. With reference to the load level required for the initiation of damage, a slightly inhibitive effect of the external secondary tensile load against failure, versus an accelerative effect of the external secondary compressive one, is predicted. A detailed description of all these alterations can be found in Correa et al. [23].

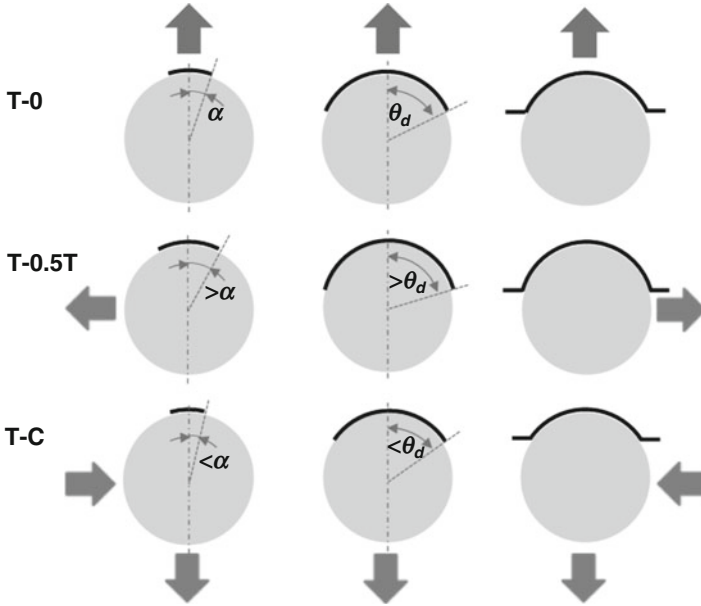


Fig. 14.13 Qualitative comparison of the phases of the mechanism of damage for different combinations of bidimensional loading under a reference tension

14.4.2 Under Compression

A parallel scheme to that employed in Sect. 14.4.1 for tension will now be developed for compression. Further details of the study summarized in this section can be found in Correa et al. [10, 24, 25].

In this section the configuration under investigation that is going to be analysed by BEM is shown in Fig. 14.14, which includes, similarly to what was considered in Fig. 14.8, not only the debonding between fibre and matrix but also a potential abandon of the fibre–matrix interface, which is kinking into the matrix.

The first question is to identify the location at which the damage may start. In the case of tension studied in Sect. 14.4.1 this location was immediate, whereas in this one is more complicated as there are no significant tension stresses normal to the interface, the shear stresses being the most significant stresses along the interface. As these stresses reach their maximum value for angles $\alpha = 45^\circ$, 135° , 225° and 315° , none of them seems to be the most plausible location of the beginning of the damage. In this study the location $\alpha = 135^\circ$ has been selected.

Once the onset of the damage has been identified, then a similar procedure than in Sect. 14.4.1 is going to be followed. Thus, an initial debonding of 10° centred at $\alpha = 135^\circ$ (a debonding between 130° and 140°) is going to be studied by a BEM model. Figure 14.15 shows the morphology of the crack under the application of the compressive load.

Fig. 14.14 Model of the damage in a single fibre under compression once the debonding crack kinks and penetrates into the matrix

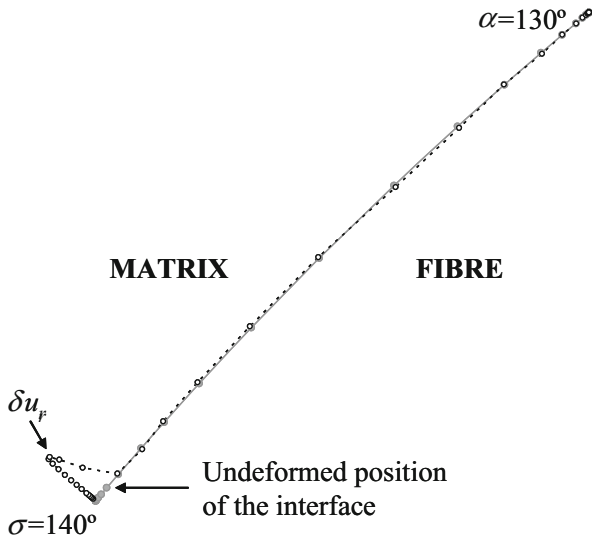
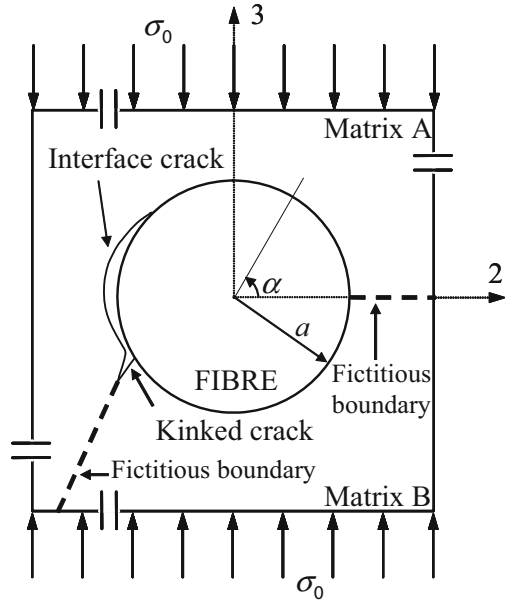


Fig. 14.15 Morphology of the incipient debonding crack under compression represented by the radial displacements of the lips of the debonding crack

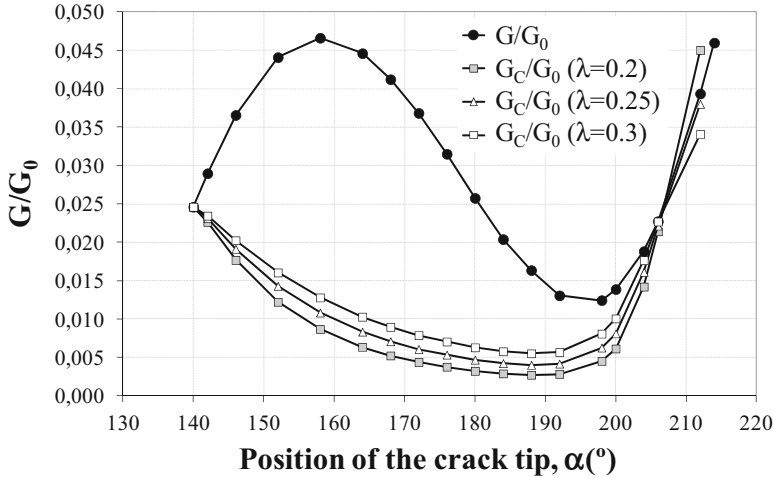


Fig. 14.16 Evolution of G and G_C for the debonding crack under compression as a function of the semidebonding angle

The BEM predictions of the morphology of the crack indicate that, in accordance with what was explained in Fig. 14.1, there is a closure of the lips at the top tip, indicating that the fracture growth is at this tip controlled by the contact model. On the contrary, the presence of a bubble is detected at the bottom tip of the incipient debonding crack, indicating that the fracture growth is in this case controlled by the open model.

This information leads to consider that the crack will propagate from the tip placed at 140° (under a mixed mode with significant participation of mode I) instead of propagating at the tip placed at 130° (under a pure mode II). In accordance with this idea the evolution of G is now investigated, and for the sake of brevity, only the total values of G will be shown, see Fig. 14.16.

The inspection of the predictions shown in Fig. 14.16 leads to conclude that the incipient debonding crack would grow in an unstable manner until an angle α in between 200° and 210° , slightly depending on the material parameter λ , stopping the growth at this position.

The next step now is to investigate the stress state in the neighbourhood of the tip of the debonding crack once it has stop. As in Sect. 14.4.1, the criterion taken to establish the direction of kinking is that based on the maximum circumferential stress. Figure 14.17 represents in this case the direction of maximum circumferential stress σ_θ in accordance with a BEM model for two physically relevant values of the radius at which the calculations are performed. The analytical predictions based on the Comninou contact model are also included for comparison.

It is now relevant to mention that in Sect. 14.4.1 the key point connecting the analysis of the evolution of the damage at micromechanical level, as well as the observed damage at mesomechanical level, i.e., the apparent plane of failure of the

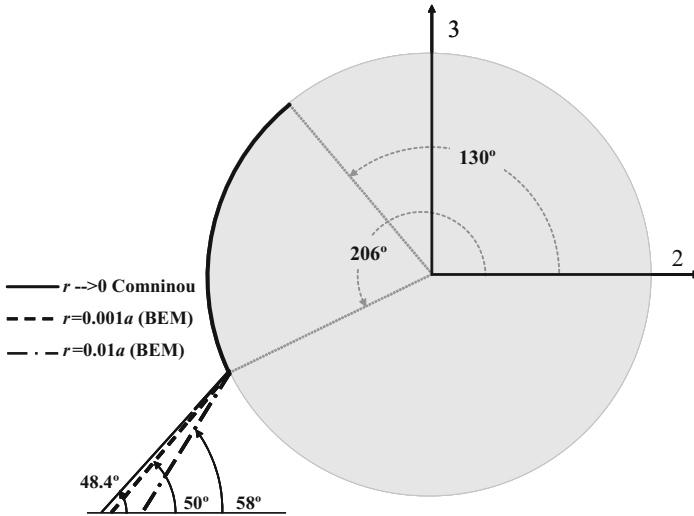


Fig. 14.17 Comparison between prediction of maximum circumferential stress for physically relevant radii based on BEM and analytical predictions based on contact fracture model

lamina, was the direction of maximum circumferential stress at which the debonding crack abandoned the fibre-matrix interface, kinking into the matrix. In the case studied in Sect. 14.4.1 this direction was that normal to the load applied. Following now a similar reasoning, the expected apparent angle of failure would be one of an order in between 50° and 58° .

Figure 14.18 shows a picture of the final configuration of the broken specimen, indicating that the apparent plane of failure found in practice is in the indicated order, 55° in the case shown, which is clearly within the range found in the predictions. This evidence is a clear confirmation of the role that micromechanics can play in predicting the behaviour of composites as an equivalent homogeneous material.

All of this leads to consider that the growth of the damage could be visualized by the scheme shown in Fig. 14.19, under the reference $C = 0$. The influence of the presence of another transversal loading is also represented in Fig. 14.19 under the reference $C = 0.1T$ for the case of the superposition of a transversal tension with a value of one tenth of the reference compression, and under the reference $C = 0.5C$ for the case of the superposition of a transversal compression with a value of one half of the reference compression.

In general terms, it can be observed that the main alterations when a transverse loading appears in a failure dominated by compression are an accelerative effect of the external secondary tensile load on failure versus an inhibitive effect of the external secondary compressive one. In particular, larger lengths of interfacial growth are found as the secondary tension increases, whereas shorter lengths are predicted for the compressive case. In fact, these results justify the selection of the particular cases in the figure, as a sufficient secondary tension increase could turn

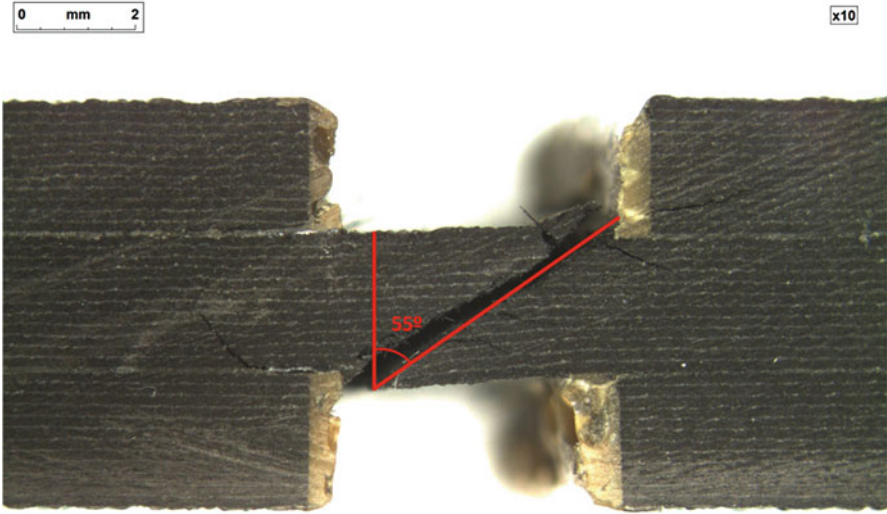


Fig. 14.18 Scheme of the failure of a specimen under compression normal to the direction of the fibre

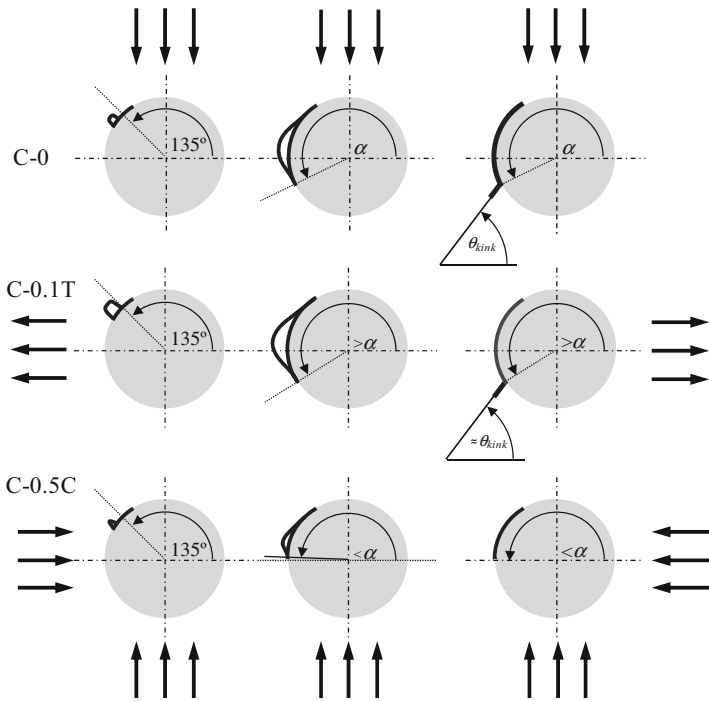
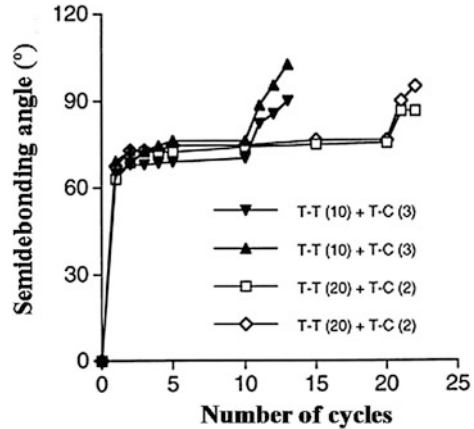


Fig. 14.19 Qualitative comparison of the phases of the mechanism of damage for different combinations of bidimensional loading under a reference compression

Fig. 14.20 Semidebonding angle with respect to the number of loading cycles in tension–tension ($T - T$) followed by tension–compression cycles ($T - C$)



the propagation into the mechanism of damage under tension, whereas a sufficient secondary compression could limit the crack growth just to the interface. A detailed description of these alterations can be found in Correa et al. [25].

14.5 Micromechanics in Fatigue Loading

Another parcel where Micromechanics has been able to play a clarifying role is fatigue loading in the direction transverse to the fibres.

Gamstedt and Sjogren [26] had found that the debonding between a single fibre and its surrounding matrix grew under certain combinations of tension and compression cycles, a fact not easy to explain.

These experimental observations seemed to indicate, Fig. 14.20, that after several $T - T$ cycles, the debonding angle maintained an almost constant value of $60^\circ - 70^\circ$. However, entering into $T - C$ cycles led to increase the debonding angle.

To give an explanation of this fact, again a comparative study between the evolution of G and G_C with the debonding angle was carried out. Figure 14.21 shows this evolution using in this case two values of the parameter λ and starting the study from the debonding observed after the $T - T$ cycles, assuming that the conditions for any additional debondings are fulfilled.

The evolutions shown in Fig. 14.21 support the observed phenomenon that excursions into $T - C$ cycles produce an increase in the debonding angle (reaching a position closed to 100°), which can lead to the appearing of a generalized level of damage at macromechanical level in a laminate.

14.6 The Role of Residual Stresses

The role of residual stresses associated with the curing process is very well known and its effects understood at mesomechanical level, these stresses being involved in the design of a structural component. The reason for the appearance of these

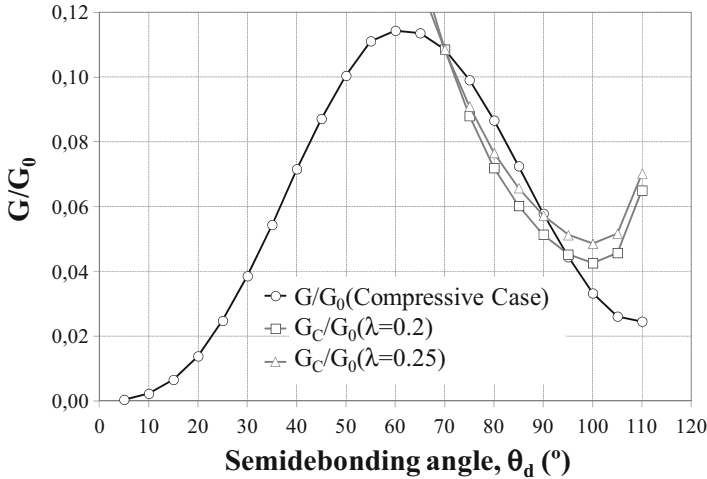


Fig. 14.21 Evolution of G and G_C along the $T-C$ cycle as a function of the semidebonding angle

residual stresses is the different values of the expansion coefficient α of a ply in the direction of the fibres as well as in the direction perpendicular to the fibres. Obviously, what is at the root of this problem are the different values of the thermal expansion coefficient of fibre and matrix.

However, not too much attention has been paid to the effect of curing on the generation of residual stresses at micromechanical level and the consequences that this fact may have on the performance of a composite, see nevertheless a pioneering study by Paris et al. [27].

This question is going to be studied in this section at micromechanical level. The effect will be studied first under tension, shown in Sect. 14.6.1, and then under compression, shown in Sect. 14.6.2. In both cases, predictions based on numerical BEM analysis and using a simple single fibre model are generated, the predictions being ratified by appropriate tests.

14.6.1 Under Tension

Having in mind the different phases of the appearance of damage transverse to the fibres under tension (nucleation of an incipient debonding crack, propagation of this debonding crack, kinking and penetration into the matrix), it is believed that the one being mainly affected by the generation of residual stresses at micromechanical level has to be necessarily the debonding between the fibre and the matrix, as there is a stress state originated by curing acting on the interface along which the debonding will take place.

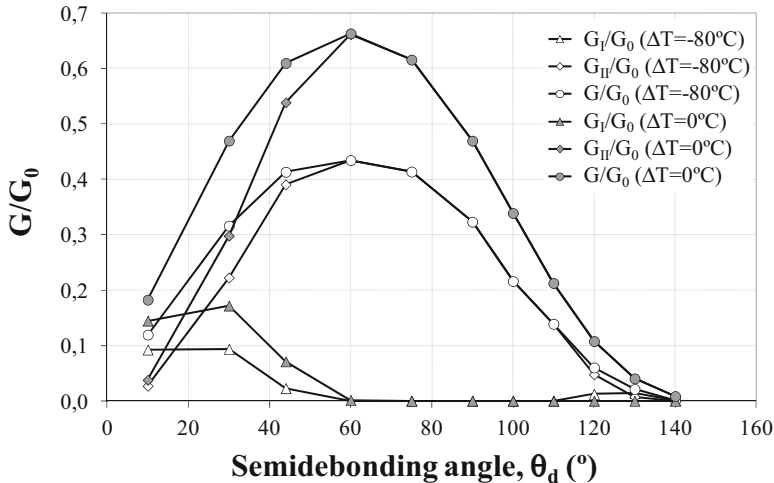


Fig. 14.22 G evolutions versus the debonding angle of a glass fibre system under tension for two curing conditions

The distribution of G versus the debonding angle has been studied for two different situations of curing, one considering a cooling of $\Delta T = -80^\circ\text{C}$ and the other one without considering it, i.e., $\Delta T = 0^\circ\text{C}$, see Fig. 14.22.

The evolutions of G and corresponding parts G_I and G_{II} for the two values of ΔT studied are very similar qualitatively speaking, but it can be easily noticed how the presence of residual stresses ($\Delta T = -80^\circ\text{C}$) produces a protective effect on the interface, against the onset and progression of a debonding crack along it.

No significant variations were observed by the presence of curing stresses in the other phases of the damage, Correa et al. [28].

Experimental tests were designed to check the adequacy of the predictions. To this end, two cycles of curing were designed for a carbon composite, Cycle 1 being the recommended by the supplier of the pre-preg and Cycle 2 having a significant decrease in the temperature of curing, both with reference to a 12-ply unidirectional graphite-epoxy laminate:

- Cycle 1: heat to 121°C in 30', hold at 121°C for 1 h, heat to 177°C in 30', hold at 177°C for 3 h and cool to room temperature.
- Cycle 2: heat to 121°C in 30', hold at 121°C for 48 h and cool to room temperature.

With reference to the results found in terms of the strength of the laminates, a mean value of 38.4 MPa, with standard deviation of 4.9 MPa, was found for the composite corresponding to cycle 2, with a curing temperature of 121°C , whereas

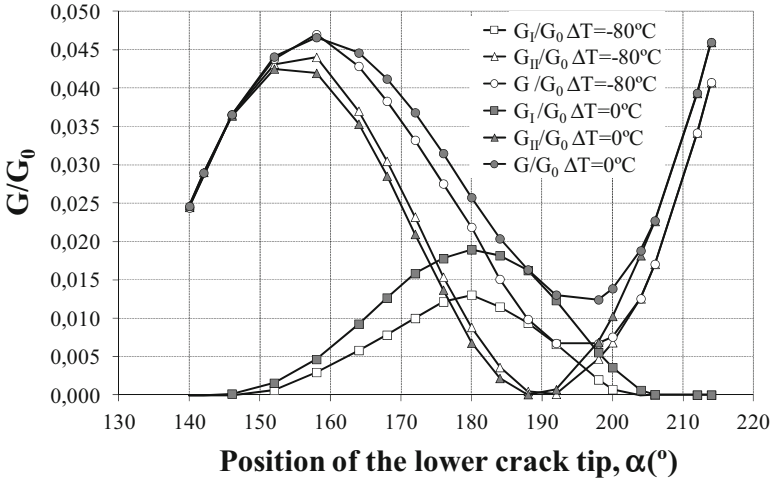


Fig. 14.23 G evolutions versus the debonding angle of a glass fibre system under compression for two curing conditions

a strength of 48.6 MPa was the mean strength found, with a standard deviation of 5 MPa, for the composite corresponding to Cycle 1, with a curing temperature of 177 °C. These results confirm the numerical predictions already obtained, i.e., the presence of higher residual stresses has a protective effect under conditions of transverse tension.

14.6.2 Under Compression

Similar predictions as those made in Sect. 14.6.1 for the case under tension are now made for the case under compression. Thus, Fig. 14.23 shows the evolutions of G , G_I and G_{II} for two cases of curing, one at room temperature $\Delta T = 0^\circ$ and another with a ΔT equal to -80°C .

It can be seen that although there are differences between the two cases studied, they are not quite significant, as the shape of the curves are practically equal and there are only small differences from a quantitative point of view. Thus, based on these predictions, not too many differences are expected in the implementation of experimental tests. Further details can be found in Correa et al. [29].

As in the case of tension previously studied, two curing cycles were designed to elucidate the effect on residual stresses.

- Cycle 1: heat to 177 °C in 50', hold at 177 °C for 2h and cool to room temperature.
- Cycle 2: heat to 121 °C in 30', hold at 121 °C for 54h and cool to room temperature.

In this case the value of the mean strength found for the 12-ply unidirectional graphite-epoxy laminate corresponding to Cycle 1 was 220 MPa, with a standard deviation of 22 MPa, whereas for the laminate cured with Cycle 2 the mean strength was 212 MPa, with a standard deviation of 11 MPa. The proximity of these two results confirms the numerical predictions in the sense that the micromechanical residual curing stresses do not play a significant role under a compression loading.

14.7 Other Studies

All the results presented till this moment correspond to the case of a single fibre embedded in a matrix under different types of loading. Two questions of different nature are now going to be studied. The first refers to the case of considering a secondary fibre in the neighbourhood of the damaged fibre, while the second refers to the micromechanical view of the *scale effect* in composites.

14.7.1 The Role of a Secondary Fibre

All the studies shown so far in this chapter correspond to a single fibre embedded in a matrix. In this section the study will be extended to the presence of a second fibre to see if the results associated with the new situation considered may offer information about the local weakness of the composite due to its heterogeneous nature.

To this end, the new configuration shown in Fig. 14.24 is going to be studied again using a BEM model. As shown in the figure, there is a central fibre presenting a debonding crack and a secondary fibre which orientation with respect to the damaged fibre is defined by the distance r_2 and the angle θ_2 .

The interest is again focused on studying the evolutions of the ERR by the debonding crack, yet now with an emphasis in how the position of the secondary fibre alters these evolutions. A detailed description of this question can be found in Sandino et al. [30]. Here, to summarize, a particular attention will be devoted to a couple of questions that are representative of the damage under consideration, that corresponding to the debonding between fibre and matrix.

First of all, the extension of the damage versus the position of the secondary fibre in terms of the angle θ_2 is studied as seen in Fig. 14.25 for a fixed position of the secondary fibre ($r_2 = 2.4 r_1$). The end of unstable growth corresponding to the single fibre case is taken as a reference, representing the same feature, the end of unstable growth, for different positions of the secondary fibre.

The information obtained from Fig. 14.25 is represented by means of a graph, to facilitate its comprehension, in Fig. 14.26.

Thus, it can be seen from Fig. 14.26 that the positions of the secondary fibre marked in red correspond to configurations to which the extension of the damage is

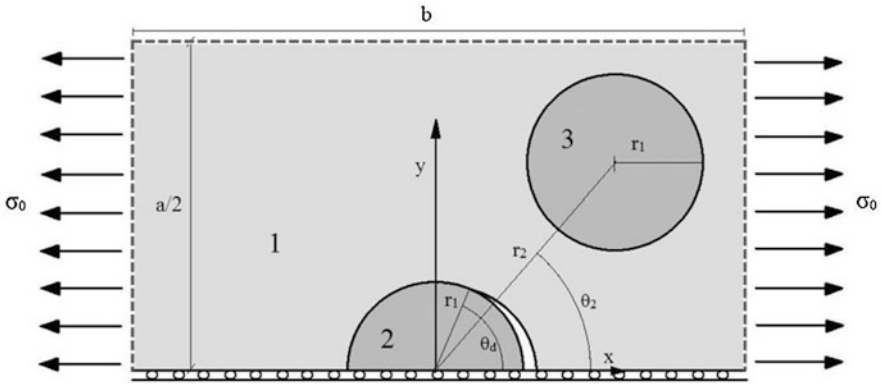


Fig. 14.24 Model including a primary fibre with an interface crack and an undamaged secondary fibre

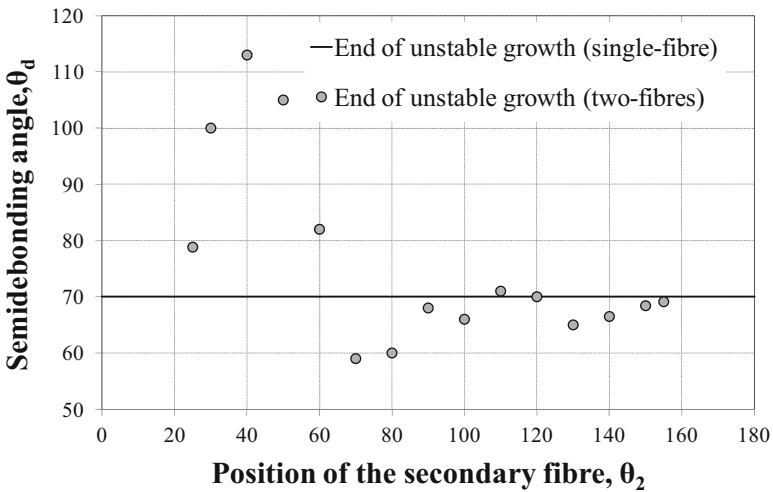


Fig. 14.25 End of unstable growth of the debonding crack versus the position of the secondary fibre

greater, see quantitatively this effect in Fig. 14.25. On the contrary, those positions marked in green correspond to configurations in which the extension of the unstable growth is smaller, see quantitatively this effect in Fig. 14.25. Those positions marked in black correspond to configurations where the end of unstable growth is not affected by the position of the secondary fibre.

The second question studied is the effect of the position of the secondary fibre in the amount of energy released by the debonding crack. In this sense, the value of G associated with the first debond considered, i.e., $\theta_d = 10^\circ$ in this case, could be chosen as a representative parameter of the mechanism of damage at micromechanical level, in order to establish a connection between the micro- and

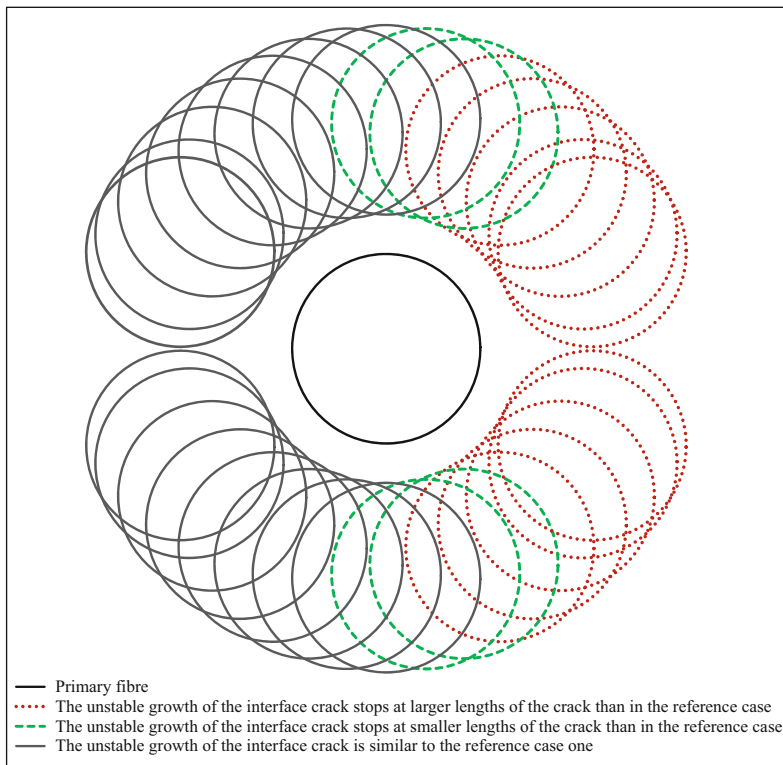


Fig. 14.26 Graph showing the effects of the presence of the secondary fibre on the extension of the unstable growth

macro-mechanical level, Correa et al. [28]. Thus, a comparison between the value of the ERR G for a fixed initial semidebonding of 10° associated with different values of θ_2 is presented in Fig. 14.27.

It can be clearly seen how positions of the secondary fibre aligned with the primary fibre produce higher values of G . A particular attention is required to understand the case of θ_2 equal to 0° (the secondary fibre is aligned with that under consideration and ahead of the location where the debonding is going to take place), as the high value of G obtained has required the use of a different scale near θ_2 equal to 0° , see Fig. 14.27.

The explanation of this fact is that the opening mode of the debonding crack (i.e. the mode I associated with the growth of the debonding) is dominant for small values of the debonding and is conditioned by the stiffness of the material occupying the area ahead of the zone where the debonding is going to take place. Thus, the area

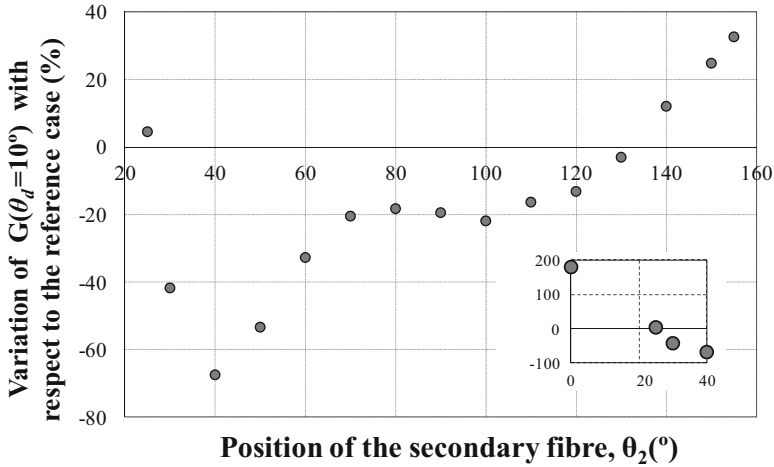


Fig. 14.27 Variation of $G(\theta_d = 10^\circ)$ versus θ_2 in relation to the reference case with detail for $\theta_2 = 0^\circ$

occupied by the stiff material (glass in this case) represented by the fibre forces the crack to open much more than in the case in which the matrix, less stiff, occupies the same area, then giving rise to a greater value of G .

A summary of the results shown in Fig. 14.27 is represented in Fig. 14.28 where positions of the fibres in red would correspond to positions where a higher level of load is required for an incipient crack to propagate, whereas those in green would correspond to positions where a smaller level of load is required. Thus, in simple terms, positions in red would represent an accelerative effect on the appearance of debonding, whereas those in green would represent a retardant effect in terms of appearance of the debonding.

With regards to the distance between the fibres, it is observed that most effects disappear for $r_2/r_1 = 2.5$, although the disappearance of the totality occurs for $r_2/r_1 = 7$.

14.7.2 Scale Effect at Micromechanical Level

What has been known as scale effect in composites, based on experimental evidences, see Parvizi et al. [31] and Flagg and Kural [32] among others, refers basically to the variable apparent strength that a lamina has, depending on several questions such as the thickness of the lamina or the orientations of the adjacent laminas.

Different explanations have been given to this fact, the most recent being based on the double stress and energy criteria, García et al. [33], which gives a very accurate prediction of experimental results by Parvizi et al. Based on Finite Fracture

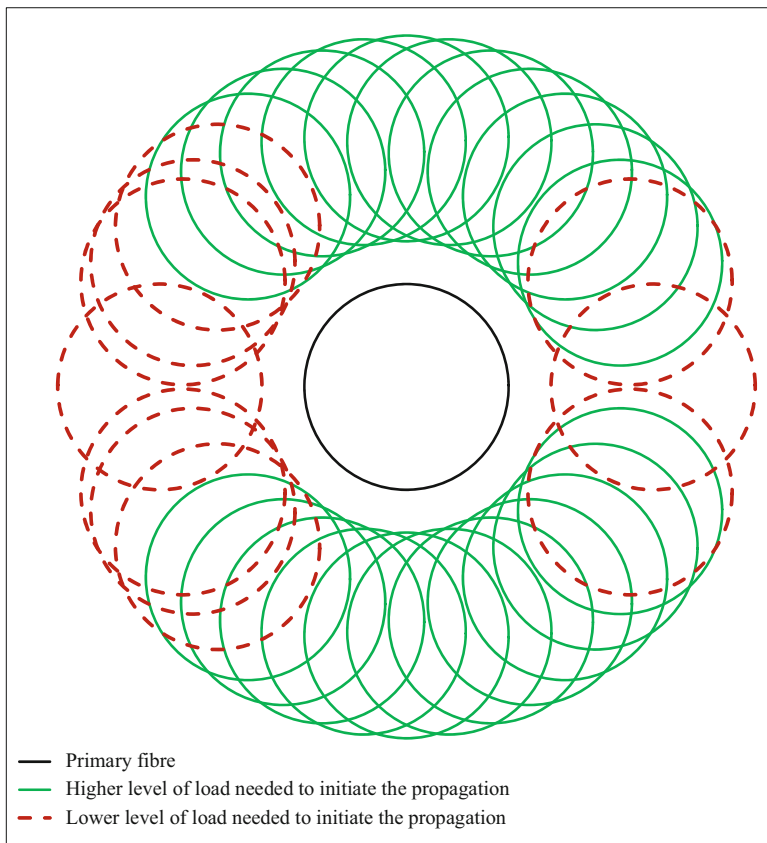


Fig. 14.28 Graph of the effects of $G(\theta_d = 10^\circ\text{C})$ versus failure

Mechanics (FFM), Mantič [34], this view of the problem gives a minimum size of the expected damage in a weak lamina (typically 90° lamina). As the predictions are based on a mesomechanical view of the problem, it will be reviewed in this chapter from a micromechanical point of view.

The configuration now studied, represented in Fig. 14.29, Velasco et al. [35], corresponds to a $[0, 90n]_S$ laminate, and a double scale model, based again in BEM, is going to be carried out. The outer 0° lamina ($t_0 = t_{90} = 170\ \mu\text{m}$) is modelled at a mesoscale level with an orthotropic behaviour in the transversal longitudinal plane under consideration, plane xy in Fig. 14.29. The central 90° lamina is also considered at a mesoscale level having isotropic behaviour in the plane under consideration. This 90° lamina includes a micromechanical cell in which a fibre ($7.5\ \mu\text{m}$ of diameter) surrounded by matrix is modelled, maintaining the fibre volume (55%) of the composite.

The properties of the four materials involved in the model are given in Table 14.2.

Table 14.2 Elastic properties of the materials involved in the multiscale model

Material	Properties
0° ply (orthotropic)	$E_{11} = 135 \text{ GPa}$, $E_{22} = 8.75 \text{ GPa}$, $E_{33} = 8.75 \text{ GPa}$, $\nu_{12} = 0.3$, $\nu_{13} = 0.3$, $\nu_{23} = 0.4$, $G_{12} = 4.75 \text{ GPa}$
90° ply (isotropic)	$E(E_{22} = E_{33}) = 8.75 \text{ GPa}$, $\nu = 0.3$
Matrix (epoxy, isotropic)	$E = 4.2 \text{ GPa}$, $\nu = 0.32$
Fibre (carbon, isotropic)	$E(E_{22}) = 15 \text{ GPa}$, $\nu = 0.2$

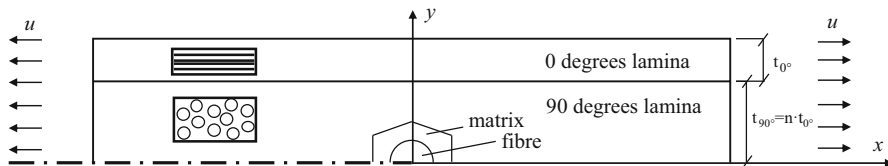


Fig. 14.29 Multiscale BEM model of a $[0, 90n]_S$ laminate

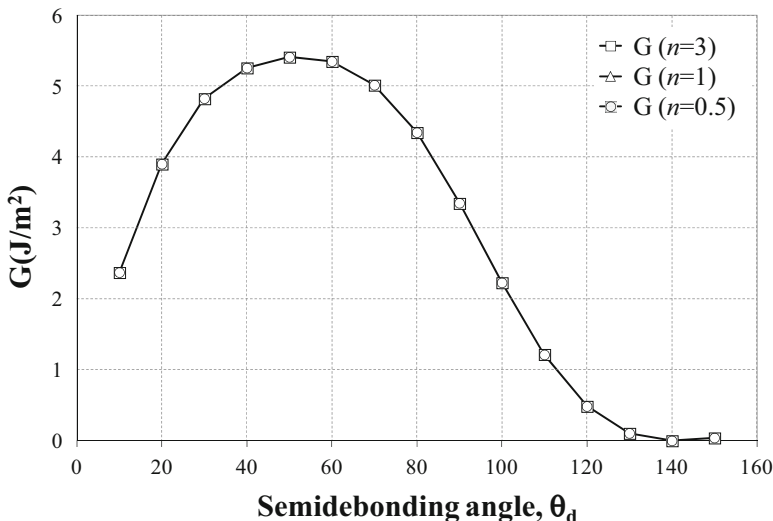


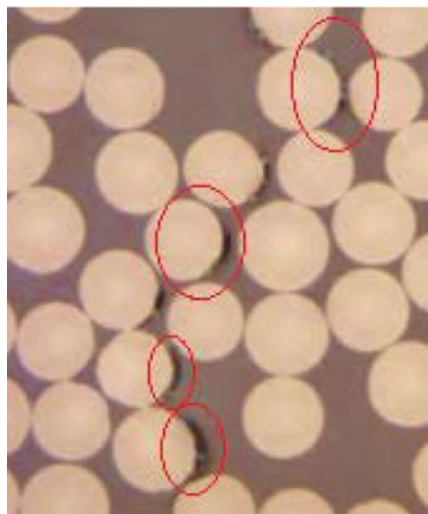
Fig. 14.30 Scale effect on the values of the ERR G corresponding to a debonding crack between the fibre and the matrix

Now the question is to see the influence that the scale effect (the value of n in the laminate) has on the main mechanism of interfibre damage: the debonding between the fibre and the matrix. To this end, the evolution of G as a function of the debonding angle is going to be studied for different values of n . Figure 14.30 shows such evolution for $n = 0.5, 1, 3$.

Figure 14.30 clearly shows, due to the coincidence of the evolutions of G for the three values of n studied, that the damage under consideration is not affected at all by the scale effect (for the sake of brevity only the total value of G is represented, not having found any difference neither in G_I nor in G_{II}). The appearance of this damage would then be connected to the ‘quality’ of the interface/interphases between the fibre and the matrix. Thus, a similar level of external loading ought to lead to a similar level of damage, if any, of this type.

First of all the appearance of this damage is widely observed in the literature and has been also detected by the authors, see Fig. 14.31.

Fig. 14.31 Micrography of debondings associated with transverse failure



Looking for a specific correlation with the scale effect, Saito et al. [36] show the presence of this type of damage, isolated debonding between the fibre and the matrix with equivalent morphology, for two laminates with different values of the parameter n , and at the same level of loading.

14.8 Conclusions

A study on the interfibre failure based on Micromechanics has been carried out in this chapter. A single fibre model embedded in matrix has been used to investigate the onset and growth of the phase of the mechanism considered to be of major importance in the interfibre failure, the debonding between the fibre and the matrix. The problem has been studied using the approaches associated with Interfacial Fracture Mechanics, and using BEM as the most appropriate tool to deal with a problem involving singular stress states and non-linear features derived from the contact between debonded surfaces of fibre and matrix.

First of all, a micromechanical study has been conducted to clarify the question of adopting the stress vector at mesomechanical level associated with a plane as the entity responsible for the interfibre failure at this plane. A micromechanical explanation has been given, showing the involvement in the failure of stress components non-associated with this stress vector. The numerical predictions have been supported by experimental tests involving lateral precompressions on specimen under tension transverse to the fibres.

The morphologies of the damage found under tension and compression have been explained by means of micromechanical analyses, establishing the correlation between the predictions and the experimental observations. The effect of superimposing a lateral transverse load to the nominal transversal one has also been studied.

The role of micromechanical curing residual stresses has been investigated using again a BEM model. The predictions showed a significant influence of these residual stresses under transverse tension and almost no influence under transverse compression. Different manufacturing procedures were tried to obtain materials with similar properties but curing with different temperatures. Transverse testing under tension and compression corroborates the predictions, showing that residual stresses play a protective effect under tension, not having any relevant role under compression.

An excursion to a more complicated model involving a secondary fibre has also been carried out, identifying the configurations that precipitate or delay the appearance of failure, under tension and under compression.

Finally, the well-known size effect has been visited from a micromechanical point of view. It has been proven that there is no size effect for the appearance of an isolated debonding of a fibre from the matrix. In other words, similar damage at this micromechanical level ought to be observed for a certain level of load, regardless the origin of the scale effect, the thickness of the lamina that affects the failure, which has given rise to the in-situ strength concept.

It has to be said that the model used in most of the cases is a very simple one involving a single fibre. It could be argued that it is quite simple to model all the possibilities one fibre may find in an actual laminate. However, in the light of the information obtained with this simple model versus others that are more complicated, involving a complete generation and propagation of damage, one may say that only physical properties associated with foundations of Fracture Mechanics are used, fitting properties of a model not being required. It is also important to mention that the purpose of the analysis carried out is not to establish predictions on strength but to understand the mechanisms of failure that may help to design composites with improved performance, as well as to be able to propose physically based failure criteria.

Acknowledgements This study was supported by the Spanish Ministry of Education and Science/Economy and Competitiveness and the Junta de Andalucía (Projects MAT2013-45069-P, DPI 2012-37187 and P11-TEP-7093).

References

1. R. Jones, *Mechanics of Composite Materials* (McGraw-Hill, New York, 1975)
2. S.W. Tsai, H.T. Hahn, *Introduction to Composite Materials* (Technomic, Southampton, 1980)
3. B.D. Agarwal, L.J. Broutman, *Analysis and Performance of Fibre Composites* (Wiley, New York, 1980)
4. J.C. Halpin, *Primer on Composite Materials*, 2nd edn. (Technomic, Lancaster, PA, 1992)

5. F. París, A study of failure criteria of fibrous composite materials. NASA/CR-2001-210661 (2001)
6. M.L. Williams, The stress around a fault of crack in dissimilar media. *Bull. Seismol. Soc. Am.* **49**, 199–204 (1959)
7. M. Comninou, The interface crack. *J. Appl. Mech.* **44**, 631–636 (1977)
8. V. Mantič, A. Blázquez, E. Correa, F. París, Analysis of interface cracks with contact in composites by 2D BEM, in *Fracture and Damage of Composites*, ed. by M. Guagliano, M.H. Aliabadi (WIT, Southampton, 2006), pp. 189–248
9. F. París, E. Correa, V. Mantič, Kinking of transversal interface cracks between fiber and matrix. *J. Appl. Mech.* **74**, 703–716 (2007)
10. E. Correa, V. Mantič, F. París, Numerical characterisation of the fibre–matrix interface crack growth in composites under transverse compression. *Eng. Fract. Mech.* **75**(14), 4085–4103 (2008)
11. M.Y. He, J.W. Hutchinson, Kinking of a crack out of an interface. *J. Appl. Mech.* **56**, 270–278 (1989)
12. J.W. Hutchinson, Z. Suo, Mixed mode cracking in layered materials. *Adv. Appl. Mech.* **29**, 63–191 (1992)
13. F. París, J. Cañas, *Boundary Element Method. Fundamentals and Applications* (Oxford University Press, Oxford, 1997)
14. E.K. Gamstedt, Fatigue damage mechanisms in polymer matrix composites. Ph.D. thesis, Lulea University of Technology (1997)
15. Z. Hashin, A. Rotem, A fatigue failure criterion for fiber reinforced materials. *J. Compos. Mater.* **7**, 448–64 (1973)
16. A. Puck, H. Schurmann, Failure analysis of FRP laminates by means of physically based phenomenological models. *Compos. Sci. Technol.* **58**, 1045–1067 (1998)
17. C.T. Sun, B.J. Quinn, J. Tao, D.W. Oplinger, Comparative evaluation of failure analysis methods for composite laminates. DOT/ FAA/AR-95/109 (1996)
18. M. Toya, On mode I and mode II energy release rates of an interface crack. *Int. J. Fract.* **56**, 345–352 (1992)
19. Y. Murakami, *Stress Intensity Factor Handbook* (Pergamon, Oxford, 1988)
20. F. París, E. Correa, J. Cañas, Micromechanical view of failure of the matrix in fibrous composite materials. *Compos. Sci. Technol.* **63**, 1041–1052 (2003)
21. V. Mantič, F. París, Relation between SIF and ERR based measures of fracture mode mixity in interface cracks. *Int. J. Fract.* **130**, 557–569 (2004)
22. F. Erdogan, G.C. Sih, On the crack extension in plates under plane loading and transverse shear. *J. Basic Eng.* **85**, 519–527 (1963)
23. E. Correa, V. Mantič, F. París, Effect of the presence of a secondary transverse load on the inter–fibre failure under tension. *Eng. Fract. Mech.* **103**, 174–189 (2013)
24. E. Correa, V. Mantič, F. París, A micromechanical view of inter–fibre failure of composite materials under compression transverse to the fibres. *Compos. Sci. Technol.* **68**(9), 2010–2021 (2008)
25. E. Correa, F. París, V. Mantič, Effect of a secondary transverse load on the inter–fibre failure under compression. *Compos. Part B* **65**, 57–68 (2014)
26. E.K. Gamstedt, B.A. Sjøgren, Micromechanisms in tension–compression fatigue of composite laminates containing transverse plies. *Compos. Sci. Technol.* **59**(2), 167–78 (1999)
27. F. París, J.C. del Caño, J. Varna, BEM analysis of the contact problem in fibres debonded of a matrix. Effect of curing stresses, in *Boundary Elements XX*, ed. by A. Kassab, C.A. Brebbia, M. Chopra (Computational Mechanics Publications, Southampton, 1998), pp. 145–156
28. E. Correa, V. Mantič, F. París, Effect of thermal residual stresses on matrix failure under transverse tension at micromechanical level: a numerical and experimental analysis. *Compos. Sci. Technol.* **71**(5), 622–629 (2011)
29. E. Correa, F. París, V. Mantič, Effect of thermal residual stresses on the matrix failure under transverse compression at micromechanical level: a numerical and experimental study. *Compos. Part A* **43**(1), 87–94 (2012)

30. C. Sandino, E. Correa, F. París, Numerical analysis of the influence of a nearby fibre on the interface crack growth under transverse tensile load. *Eng. Fract. Mech.* (2016). <http://dx.doi.org/10.1016/j.engfracmech.2016.01.022>
31. A. Parvizi, K.W. Garret, J.E. Bailey, Constrained cracking in glass fibre-reinforced epoxy cross-ply laminates. *J. Mater. Sci.* **13**, 195–201 (1978)
32. D.L. Flagg, M.H. Kural, Experimental determination of the in situ transverse lamina strength in graphite/epoxy laminates. *J. Compos. Mater.* **16**(2), 103–116 (1982)
33. I.G. García, V. Mantič, A. Blázquez, F. París, Transverse crack onset and growth in cross ply $[0/90]_S$ laminates under tension. Application of a coupled stress and energy criterion. *Int. J. Solids Struct.* **51**, 3844–3856 (2014)
34. V. Mantič, Interface crack onset at a circular cylindrical inclusion under a remote transverse tension. Application of a coupled stress and energy criterion. *Int. J. Solids Struct.* **46**, 1287–304 (2009)
35. M.L. Velasco, F. París, J.C. Marín, J. Justo, A. Barroso, E. Graciani, Numerical and experimental study on the failure of non-conventional laminates, in *ECCM17—European Conference on Composite Materials*, Munich (2016)
36. H. Saito, H. Takeuchi, I. Kimpara, Experimental evaluation of the damage growth restraining in 90 layer of thin-ply CFRP cross-ply laminates. *Adv. Compos. Mater.* **21**, 57–66 (2012)